J. Fluid Mech. (1996), *vol.* 313, *pp.* 381–407

Convective instability in rotating liquid ^{3}He–^{4}He mixtures

By M. S. THURLOW[1], B. J. BROOKS[2], P. G. J. LUCAS[3]†, M. R. ARDRON[4], J. K. BHATTACHARJEE[5] AND A. L. WOODCRAFT[3]

[1] Forecasting Research, Meteorological Office, Bracknell, Berkshire, RG12 2SZ, UK

[2] School of Physics, University of Bath, Bath, BA2 7AY, UK

[3] Department of Physics and Astronomy, The University, Manchester M13 9PL, UK

[4] Department of Chemical and Process Engineering, Merz Court, The University, Newcastle on Tyne, UK

[5] Department of Physics, Indian Institute of Technology, Kanpur 208016, India

(Received 20 March 1995 and in revised form 30 August 1995)

Thermal convection is investigated experimentally in a dilute liquid mixture of ^{3}He in ^{4}He at four temperatures between 20 and 100 mK above the superfluid transition temperature, chosen for their proximity to the codimension-two and hydrodynamic tricritical points. Two experimental cells of aspect ratio 2.76 and 1.00 were used. For the cell with the higher aspect ratio, two convective transitions at each of the four temperatures were observed above a critical angular velocity, and only one observed below. At temperatures lower than that of the hydrodynamic tricritical point the transition with the lower critical Rayleigh number is hysteretic for all angular velocities; above this temperature hysteresis is absent. The critical Rayleigh numbers are compared with theoretical predictions that take into account the existence of convection modes with azimuthal angular dependence. In the case of the cell with the smaller aspect ratio thermal relaxation oscillations were observed when heating from below. Convective thresholds were again observed but their critical Rayleigh numbers are almost independent of angular velocity. Some suggestions are advanced for this unexpected behaviour.

1. Introduction

In this report we present a detailed account of experimental measurements of convection thresholds and convective heat transfer in a uniformly rotating horizontal cylindrical layer of dilute normal liquid mixture of ^{3}He in ^{4}He heated from below and maintained at temperatures between 20 and 100 mK above its λ-transition. An earlier, preliminary, account exists (Lucas *et al.* 1994). No other report on convection experiments on rotating binary mixtures of any kind appears to exist. However, there have been a number of papers on the theory of the subject: Antoranz & Velarde (1978, 1979); Pearlstein (1981); Bhattacharjee (1988*a*, *b*, *c*, 1989); Ardron, Lucas & Stein (1992) and Net, Mercader & Knobloch (1995). A very large literature exists on non-rotating binary mixtures: for example Mercader, Net & Knobloch (1995) describe recent progress on the linear theory of binary fluid convection in finite aspect ratio containers, while the paper by Kolodner (1994) is representative of the large body of

† Author to whom correspondence should be addressed.

experimental work on nonlinear convection in binary mixtures. Rotating homogeneous fluids have also been studied over a long period: Goldstein *et al.* (1993, 1994) summarize the current theoretical position, while Zhong, Ecke & Steinberg (1993) describe recent experiments on rotating water.

Our interest in low-temperature ^{3}He–^{4}He mixtures stems from the following facts: (*a*) only in this system are the temperature and concentration differences small enough to permit unambiguous observation of a codimension-two point and points where the convection threshold changes from forward to backward (Ahlers & Rehberg 1986; Gao & Behringer 1986; Sullivan & Ahlers 1988*a*, *b*; Onions *et al.* 1990); (*b*) the Prandtl number, of order 0.5, lies between the two extremes of liquid metals and room-temperature fluids; (*c*) it is relatively straightforward to maintain the temperature stability of the fluid sample to μK levels and lower and to reduce heat leaks to nW levels; (*d*) the heat capacity of the fluid dominates that of the components making up the experimental cell. The effect that rotation has on the codimension-two point and the forward/backward transition behaviour is of interest and Ardron *et al.* (1992) have examined the former theoretically. The present inability to visualize the flow pattern in low-temperature systems is a disadvantage compared with room-temperature fluids, although this may prove to be a possibility in the near future (Sullivan, Steinberg & Ecke 1993). Some idea of the flow pattern is obtainable using local probes as we describe in this article.

2. Background

In our present programme we used essentially the same mixture as in our earlier experiments (Onions *et al.* 1990), for which the molar concentration X of ^{3}He in ^{4}He was stated to be 0.0235. In this earlier work the line of experimental points for the threshold Rayleigh number marking the bifurcation from the conduction to the convection state exhibited a cusp at the temperature $T_{CT} = 2.21$ K which they identified with the codimension-two point first observed in a bulk mixture by Ahlers & Rehberg (1986). This point corresponds to the time-dependent threshold convection state for $T < T_{CT}$ losing stability to the stationary threshold convection state for $T > T_{CT}$, and at this point the critical Rayleigh numbers for each state are equal. Below the temperature $T_b = 2.228$ K Onions *et al.* (1990) observed that the convection threshold exhibited hysteresis so that the critical Rayleigh number was smaller for a heat-decreasing sequence than for a heat-increasing sequence. In the temperature range $T_{CT} < T < T_b$ this hysteretic behaviour occurs because the stationary convection state is achieved via a backward bifurcation (Brand, Hohenberg & Steinberg 1984; Ahlers & Rehberg 1986). When $T < T_{CT}$, depending on the temperature several such bifurcations to different time-dependent convection states may occur as described by Sullivan & Ahlers (1988*a*, *b*). For temperatures above T_b Onions *et al.* (1990) found that hysteresis disappeared within experimental error. This behaviour is similar to that observed by Ahlers & Rehberg (1986).

It has been shown theoretically (Brand *et al.* 1984; Clune & Knobloch 1992; Schöpf & Zimmermann 1993) that if S_{CT} and S_b are the separation ratios corresponding to temperatures T_{CT} and T_b respectively then it is to be expected that $S_{CT} < S_b < 0$. The separation ratio S is defined by $S = -\beta_c k_T/\beta_T T$, where $\beta_c = -(1/\rho)(\partial\rho/\partial c)_T$ is the solutal expansion coefficient, $\beta_T = -(1/\rho)(\partial\rho/\partial T)_c$ is the thermal expansion coefficient, k_T is the thermal diffusion ratio, ρ is the density, c is the mass concentration of ^{3}He in the mixture and T is the absolute temperature. Various theoretical estimates exist (Schöpf & Zimmermann 1993) for the values of S_{CT} and S_b but typically

$S_{CT} \sim -10^{-3}$, $S_b \sim -10^{-5}$. In the temperature range under discussion the separation ratio becomes monotonically less negative with increasing temperature and changes sign to positive as the temperature is increased through an estimated value of 2.223 K for a molar concentration of 0.030 (Ahlers & Rehberg 1986). This feature occurs because the thermal diffusion ratio k_T passes through zero at the same temperature and the definition of S contains k_T as a factor. Two other dimensionless fluid parameters relevant to the experiments are the Prandtl number $\sigma = \nu/D_T$ and the Lewis number $L = D/D_T$, where $\nu = \eta/\rho$ is the kinematic viscosity, $D_T = \kappa/\rho C_p$ is the thermal diffusivity, η is the viscosity, κ the thermal conductivity, C_p the specific heat and D the mass diffusion coefficient.

Since the mixture used for the experiments reported here was the same as that used by Onions *et al.* (1990), within experimental error we were able to use the information obtained by them to choose four temperatures $T_1 = 2.161$ K, $T_2 = 2.175$ K, $T_3 = 2.218$ K and $T_4 = 2.233$ K for the experiments on rotating mixtures. From their work T_1 and T_2 are both below T_{CT}, T_3 lies between T_b and T_{CT} and T_4 above T_b. Although the temperature at which S passes through zero is not known with precision because of the lack of data on k_T in this temperature region, T_4 is sufficiently high that we expect it to be the only temperature of the four at which S is positive. We anticipate that a mixture with small positive S should behave much like pure ^4He at the same temperature since then the Soret effect and thermal expansion both operate in the same sense, leading to instability when the fluid is heated from below. Net *et al.* (1995) note that their calculations for a mixture with the slightly negative value of S of -9.1×10^{-5} are close to those for a pure fluid.

In making a comparison with theory we have utilized the sine series calculation scheme of Ardron *et al.* (1992). This scheme applies to a fluid layer of infinite lateral extent and agrees well with the infinite-layer calculations of Clever & Busse (1979) and other infinite-layer calculations on rotating binary mixtures (Antoranz & Velarde 1979; Bhattacharjee 1988*b*). However, in the experiments reported here the fluid was contained within two experimental cylindrical cells with aspect ratios Γ (Γ = radius/height) which were 2.76 in one case and 1.00 in the other, rotating uniformly about their axes which were vertical. The earlier work on rotating pure ^4He (Lucas, Pfotenhauer & Donnelly 1983; Pfotenhauer, Lucas & Donnelly 1984; Pfotenhauer, Niemela & Donnelly 1987) and the theoretical work of Buell & Catton (1983) which takes into account the existence of the sidewalls demonstrated that if Γ is of order unity, the critical Rayleigh number will be depressed below the infinite-Γ calculated values because the threshold states are likely to have a dependence on the azimuthal angle. The recent experiments of Zhong *et al.* (1993) use optical shadowgraphy to visualize the symmetry of the flow state of rotating water in $\Gamma = 1$ cylindrical geometry and their results bear out the expectations of Buell & Catton (1983) that the flow patterns can depend on the azimuthal angle and that much of the flow can take place near the wall.

However, it is also clear from the shadowgraph patterns of Zhong *et al.* (1993) that the flow state can be an m-fold spiral which is not reflection symmetric and which can precess in the rotating frame. The transition from conduction to one of these non-axisymmetric convecting states is thus a Hopf bifurcation as pointed out by Goldstein & Knobloch (1991) and Ecke, Zhong & Knobloch (1992). These results are not a feature of the theory of Buell & Catton (1983) because they did not include time-dependent states as possible solutions. Recently Goldstein *et al.* (1993, 1994) have carried out a detailed set of calculations on the threshold convection states of a rotating homogeneous fluid contained within finite-Γ geometry, allowing for time dependence

and non-axisymmetric spiral patterns. These authors show that the existence of the walls allows a new class of flow states (wall modes) in which most of the flow takes place near the walls, in addition to body modes in which flow takes place throughout the fluid and which are present in the infinite layer. The flow state that is selected can depend quite delicately on Γ and the Prandtl number. Net *et al.* (1995) have recently extended the calculations of Goldstein *et al.* (1993, 1994) to cover rotating binary mixtures. The calculations of Net *et al.* (1995; also, personal communication) have been carried out for fluid parameters corresponding closely to the mixture used in the experiments reported here at temperatures T_1, T_2 and T_4 in a cylindrical container with aspect ratio 2.76. Thus in addition to the sine series calculations which, except at low angular velocities, really only provide an upper limit to the threshold Rayleigh number, we have been able to make a direct comparison with the more applicable calculations of Net *et al.* (1995; personal communication). In this comparison we utilized those of their calculations which corresponded to the realistic boundary conditions of no slip, no mass flux and fixed temperature at the upper and lower boundaries, and no slip and no radial temperature or concentration gradients at the sidewalls.

3. Experimental details

3.1. *Rotating cryostat*

The experiments reported here were all performed on the rotating cryostat described by Ardron *et al.* (1990) and its features are summarized here briefly.

The cryostat is bolted to the underside of a 2 m diameter, 2.5 cm thick disk of aluminium which can be rotated by three a.c. linear induction motors driving an annular reaction plate embedded in its perimeter. All the electronic equipment and gas-handling plumbing required to run the experiments are mounted on the top of this platform which is supported horizontally and centred laterally by air bearings. Although a small diffusion pump is on the platform, all the large rotary pumps are off-platform and vacuum connection to the on-platform plumbing is made through a concentric vacuum seal similar in design to that of Packard & Williams (1974). All the low-level electronic signals are processed on-platform by the electronics, and the processed digitized data passed to an off-platform computer via the IEEE-488 computer interface bus through a multi-way electrical slip ring.

At the bottom of the cryostat, submerged in a bath of 4.2 K liquid helium contained in a superinsulated dewar, is a vacuum can containing a ^{4}He refrigerator and the experimental cell. The ^{4}He refrigerator is a copy of the design of DeLong, Symko & Wheatley (1971) and provides a low-temperature base of 1.3 K with a refrigeration power of 10 mW which can be maintained indefinitely provided the main bath is topped up at 70 h intervals.

Since the report by Ardron *et al.* (1990), the precision of the speed control has been improved so that speed variations are now 0.25%. This has been achieved by using an optical encoder (Hohner) producing a greater number of pulses per cryostat revolution than before and also by replacing the power supply described in our earlier report by a thyristor-based commercial unit (Davy Enterprises) in which the duty cycle of a 3-phase 415 V mains supply can be varied by adjusting the firing phase angle of the thyristors. The vibrations experienced earlier when using this supply have been eliminated by improvements in the speed control system.

3.2. *Experimental cells*

The experiments to be described fall into two groups because initially we used an experimental cell (cell 1) with an aspect ratio of 2.76 designed to be roughly compatible with the earlier cryogenic experiments on rotating ^{4}He, but later changed to using experimental cell 2 with aspect ratio 1.00 because it had become clear that the effects of the non-axisymmetric modes would be enhanced by lowering the aspect ratio. The two cell designs are shown in figure 1.

Both cells have a number of common features which are described first. Both are constructed so that the liquid sample is contained within a cylindrical volume defined by two plane oxygen-free high-conductivity copper boundaries and a section of thin-wall stainless steel tubing. Thus the cells have Rayleigh–Bénard geometry. Two Allen–Bradley resistance temperature sensors R_U and R_L provide a measure of the absolute temperature of the upper and lower copper boundaries respectively; and a matched pair R_{UD} and R_{LD}, one on each boundary, are connected differentially to allow measurement of the temperature difference between the two boundaries. Electrical heaters capable of providing a few 100 μW of power are thermally attached to each boundary and are supplied with superconducting leads to eliminate power dissipation other than in the heaters. Heat dissipated in the lower boundary heater as part of the experimental procedure was measured using a 4-wire technique close to the heater. The leads to all sensors and heaters are thermally anchored to the boundary to which they are attached and, in the case of the lower boundary, anchored a second time to the upper boundary before passing to the top of the cryostat. These precautions, together with a copper radiation shield surrounding the whole cell and thermally anchored to the upper boundary reduce stray heat leaks to the lower boundary to a negligible level.

A ^{3}He vapour pressure bulb in thermal contact with the upper boundary provided a primary thermometer with an accuracy of 0.1 mK using the 1962 ^{3}He vapour pressure scale (Sherman, Sydoriak & Roberts 1964). The vapour pressure was measured using a Datametrics capacitance pressure gauge mounted on the cryostat and connected to the bulb by a stainless steel tube of sufficiently wide bore (0.12 cm) that thermomolecular pressure connections (White 1979) were unnecessary. Overall cooling of the cell was achieved by linking the upper boundary through a thermal resistance to the 1.3 K low-temperature base.

In each cell the liquid sample filling capillary is routed to a copper plug which is a press-fit into a hole drilled in the centre of the upper boundary. The liquid mixture can then enter the cell through the narrow annular gap between the plug and the hole, avoiding the discontinuity of installing the capillary directly in the upper boundary.

Turning now to the differences between the two cells, cell 1 is similar in design to that described by Lee, Lucas & Tyler (1983). The fluid-containing volume has diameter 2.48 cm and height 0.45 cm, and the aspect ratio of 2.76 is fixed since the tube defining the walls is brazed onto the copper boundaries. The stainless steel walls have thickness 0.038 cm. Thus the geometry of cell 1 is that of a simple right cylinder with the mean temperature of each horizontal boundary measurable with the resistive sensor thermally anchored to them.

The fluid-containing volume of cell 2 has diameter 1.60 cm and height 0.80 cm so that the aspect ratio is 1.00. The sidewalls are made from a cylindrical spacer tube of Vespel SP22 (Dupont) of thickness 0.787 cm, a graphite composite which is an electrical insulator and a poor thermal conductor at low temperatures. Embedded in the spacer tube and in direct contact with the fluid sample are three vertically mounted

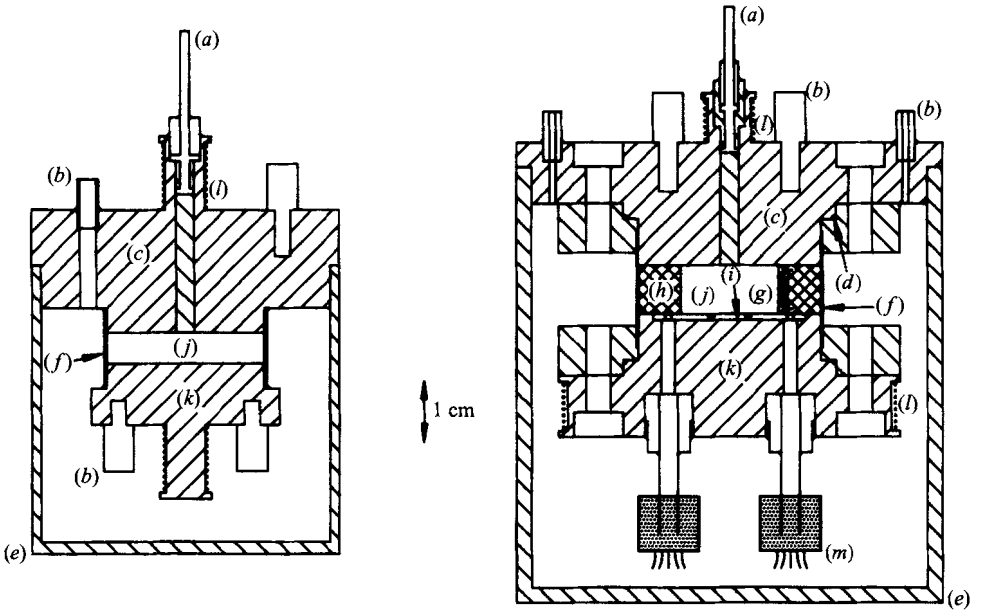

FIGURE 1. Experimental cells. (*a*) filling capillary; (*b*) thermal anchor; (*c*) upper boundary; (*d*) indium seal; (*e*) radiation shield; (*f*) stainless steel thin-wall tube; (*g*) resistive sensor; (*h*) Vespel-22 spacer; (*i*) sapphire wafer; (*j*) fluid sample; (*k*) lower boundary; (*l*) heater; (*m*) epoxy feed-through. The resistive sensors R_U, R_L, R_{UD}, R_{LD} are not shown here but are thermally anchored to the appropriate boundaries using screws and copper foil.

Allen-Bradley resistors machined flush with the tube inner surface and oriented at azimuthal angles of 0°, 28° and 49°. These sensors provide a direct measure of the temperature of the fluid with which they are in contact averaged over the cell height, at the azimuthal angle at which each is situated. The size of these sensors dictated the unusually large vertical height of the cell. A sapphire wafer glued to the lower boundary surface houses two more local sensors which unfortunately failed during use. The electrical leads for all the local sensors passed out of the fluid region through epoxy vacuum seals.

3.3. *Thermometry*

Throughout all the experiments the cell upper boundary was maintained at one of the temperatures T_1 to T_4 described in §2 to within 0.1 mK over many hours, with fluctuations being less than 10 μK over a time scale of many minutes. This temperature control was achieved by balancing the heat passing through a thermal link of thermal resistance 1000 K W^{-1} to the 1.3 K thermal base against heat supplied by the upper boundary heater. This took place under continuous negative feedback control using one of two methods. In one the upper boundary sensor R_U formed part of an a.c. ratio transformer bridge and the off-balance signal, detected by a EG&G 5210 lock-in amplifier, was used as an error signal. The R_U self-heating was kept below 10^{-7} W, this being the case also for all the other sensors. In the other method, the voltage difference between the output of the ^{3}He vapour pressure gauge and a separate voltage source was used as an error signal. Both controllers had a similar performance.

The temperature difference between the two boundaries was measured directly using a second a.c. bridge in which one arm was the differential pair R_{UD} and R_{LD} and the

other was an Ailtech programmable ratio transformer. The out-of-balance bridge signal, detected by a second lock-in-amplifier, was continually nulled by varying the ratio transformer setting using a software procedure similar to that described by Lucas & Donnelly (1981). The principle behind this instrumentation is that the ratio transformer setting is a linear function of the difference in temperature between the two boundaries and is relatively insensitive to changes in the cell mean temperature. Temperature differences can be measured to a few μK, with the bridge excitation voltage being set so that the sensors dissipate about 10^{-7} W.

The local probe sensors of cell 2 were each monitored using an a.c. resistance bridge. Unlike the other continuously balanced bridges where either a resistance value or ratio was measured, here the bridge elements other than the sensors remained fixed at values chosen to null each bridge initially. The detected out-of-balance voltages were then used as measures of the probes' subsequent temperature changes.

All the resistive sensors were temperature calibrated against the ^{3}He vapour pressure thermometer using procedures similar to that described by Lee *et al.* (1983) and the 1962 ^{3}He vapour pressure scale of Sherman *et al.* (1964).

3.4. *General instrumentation and data acquisition*

All the experiments have the common feature that the lower-boundary heater power is set to some value, or ramped or stepped in time and the resulting changes in the temperatures measured by the various sensors and local probes recorded at regular intervals (usually 10 s) over periods which could last up to 24 h. This procedure was carried out under the control of the off-platform computer which communicated with all our programmable instruments through the IEEE-488 computer interface bus.

The power developed in the lower-boundary heater was not usually more than 100 μW and was produced by a computer-controlled programmable power supply built in our laboratory and which applied a steady voltage to the heater's current leads. In series with the heater was a standard resistance through which the current passed. The potential difference both across this resistance and across the heater voltage leads were measured by a Prema programmable 10-channel potentiometric scanning multimeter to a precision of 1 μV. As well as controlling both the multimeter and the power supply, the off-platform computer used these data to perform regular calculations of the heater power.

The scanning multimeter was also used to measure the vapour-pressure thermometer gauge output and the DC output voltages from the lock-in amplifiers detecting the out-of-balance voltages of the various probe bridges. Thus the off-platform computer performed the tasks of setting the voltage across the lower boundary heater, balancing the differential resistance bridge and recording its setting, and through the scanning multimeter recording the heater power and the out-of-balance voltages of the probe bridges. Figure 2 is a schematic diagram of the data acquisition system.

3.5. *Mixture sample*

The gas mixture used for the cell 1 measurements is the identical mixture used by Onions *et al.* (1990). The method of Lee *et al.* (1983) of determining the ^{3}He molar concentration X in the liquid mixture by measuring the λ-temperature $T_\lambda(X)$ of the mixture was used both by us and by Onions *et al.* (1990). These latter authors obtained $T_\lambda = 2.139 \pm 0.001$ K while we found $T_\lambda = 2.140 \pm 0.001$ K showing that the mixture concentration had not changed within measurement error. Using a new fit

$$T_\lambda(X) = 2.1722 - 1.44842X - 0.0779809X^2 - 1.08239X^3$$

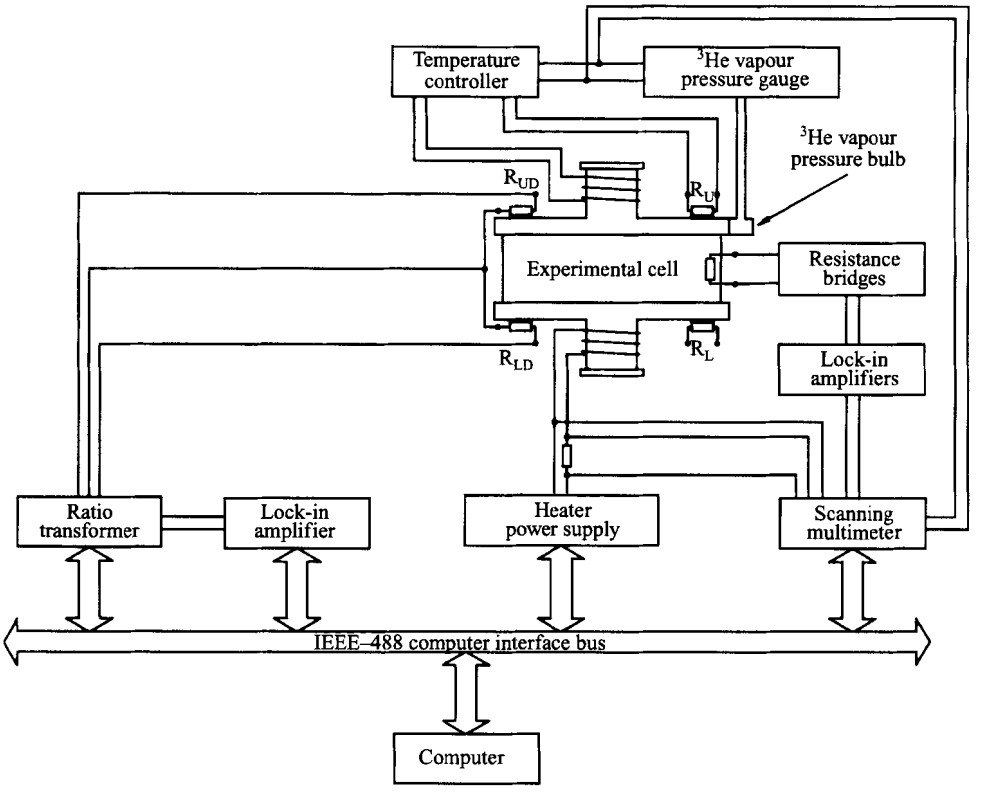

FIGURE 2. Data acquisition system.

based on the 1962 ^{3}He vapour pressure scale (Sherman *et al.* 1964) and the data on $T_\lambda(X)$ given by Sydoriak & Roberts (1960), Ryschkewitsch & Meyer (1979), Takada & Watanabe (1980) and Gestrich, Walsworth & Meyer (1984), we estimate that the molar concentration of the cell 1 mixture was $X = 0.0222 \pm 0.0007$. If this fit had been used by Onions *et al.* (1990), they would have obtained $X = 0.0229 \pm 0.0007$ rather than their stated 0.0235.

Because of unavoidable wastage of mixture in gas form between the cell 1 and cell 2 experimental programmes and also the larger volume of cell 2 it became necessary to make up some more mixture for the cell 2 experiments. We did this volumetrically, trying to achieve the same concentration, and mixed it with the original sample. A λ-point determination of this new sample when in liquid form in cell 2 yielded $T_\lambda = 2.134$ K, $X = 0.0263$, so that this sample had a slightly higher concentration with a similar experimental error in its determination to those quoted above.

The gas mixture was transferred from a gas storage volume on the platform into the cell in liquid form at 1.3 K through a 4.2 K trap to eliminate air and water vapour using a Toepler pump. Care was taken not to overfill the cell beyond a small volume just above the cell and maintained at the upper boundary temperature. This was achieved by measuring the thermal resistance between the upper and lower boundary after each stroke of the Toepler pump and discontinuing the transfer once the thermal resistance had stopped increasing. In filling the cell at 1.3 K allowance was made for the fact that the experiments were to take place at approximately 2.1 K.

4. Experiments

4.1. *Experiments with cell 1*

The aim of all the experiments was to determine the critical Rayleigh number at which there was a change in the thermal resistance of the fluid in the cell, and to examine the dependence of the Nusselt number on the Rayleigh number in the convective regime. With this cell, for which $\Gamma = 2.76$, we were looking for continuity with the previous work on pure ^{4}He by Lucas *et al.* (1983) and Pfotenhauer *et al.* (1984, 1987). Throughout, the method used was to ramp the power being dissipated by the lower-boundary heater at a constant rate while keeping the upper-boundary temperature fixed and monitoring the temperature difference between the boundaries at 10 s intervals. During the ramp the platform was kept rotating at a constant known rate. At any given upper-boundary temperature and angular velocity two consecutive ramps were made, one with heater power increasing from zero to some maximum value and then, without changing the power between ramps, one with heat decreasing from the same value to zero. The resultant plot of the bridge ratio against heater power, termed a heating curve, was a sensitive measure of changes in the heat conductance of the cell. Figures 3(*a*) and 3(*b*) are examples. The power used in these plots is the total power into the lower boundary of the cell, which includes the self-heating of the sensor R_{DL}, and it is for this reason that the plots do not start at zero on the power axis.

Figure 3(*a*) is typical, each ramp lasting 12 h, with the upper boundary of the cell at 2.161 K. During the linear part of this ramp the temperature between the cell boundaries changed at a rate of 1.33×10^{-7} K s^{-1}. The thermal diffusivity of the mixture at this temperature is 2.33×10^{-4} cm^2 s^{-1} so that the vertical thermal diffusion time is 869 s. There is thus a thermal lag of about 116 μK leading to a possible error in the determination of the critical Rayleigh number of 4.4%. This possible systematic error is about the same size as the random error in the determination of the critical Rayleigh number found experimentally when a ramp with identical experimental parameters is repeated several times. Evidence that this possible systematic error is overestimated in the calculation above is that there is very little start-up curvature visible on the heating curves.

Random fluctuations in the bridge ratio were smoothed by introducing a 21 point equal-weight sliding average, in that each bridge ratio data value was replaced by the average of the 10 data points on either side of it together with its own value. The extent of this smoothing is comparatively light since less than 1% of the data over the full power range is incorporated into each average. The data were further processed to give information on the dimensionless parameters $R = gd^3\beta_T \Delta T/\nu D_T$, the thermal Rayleigh number, and $N = W/W_{NC}$, the Nusselt number. In the definition of the Rayleigh number g is the gravitational field and ΔT is the temperature difference between the upper and lower boundaries spaced d apart. In the definition of the Nusselt number, W is the heat flow passing vertically upward through the fluid in the cell and W_{NC} the heat flow that would pass through the cell if it were not convecting. In practice W_{NC} is calculated from ΔT and the mixture thermal conductivity.

In calculating the Rayleigh number it was first necessary to convert bridge ratios to data on ΔT; this was done using the calibration obtained as described in §3.3. The data sources used for the thermodynamic and transport parameters required to calculate the Rayleigh numbers and other dimensionless numbers are Kierstead (1976) and Kakizaki & Satoh (1976) for ρ; Gestrich *et al.* (1984) for β_c, β_T, κ, k_T and D; Tuttle, Zhong & Meyer (1991) for β_T, κ and k_T; Gasparini & Moldover (1975) for C_p; Webeler & Allen (1972) and Wang, Howald & Meyer (1990) for η; and Zhong, Tuttle

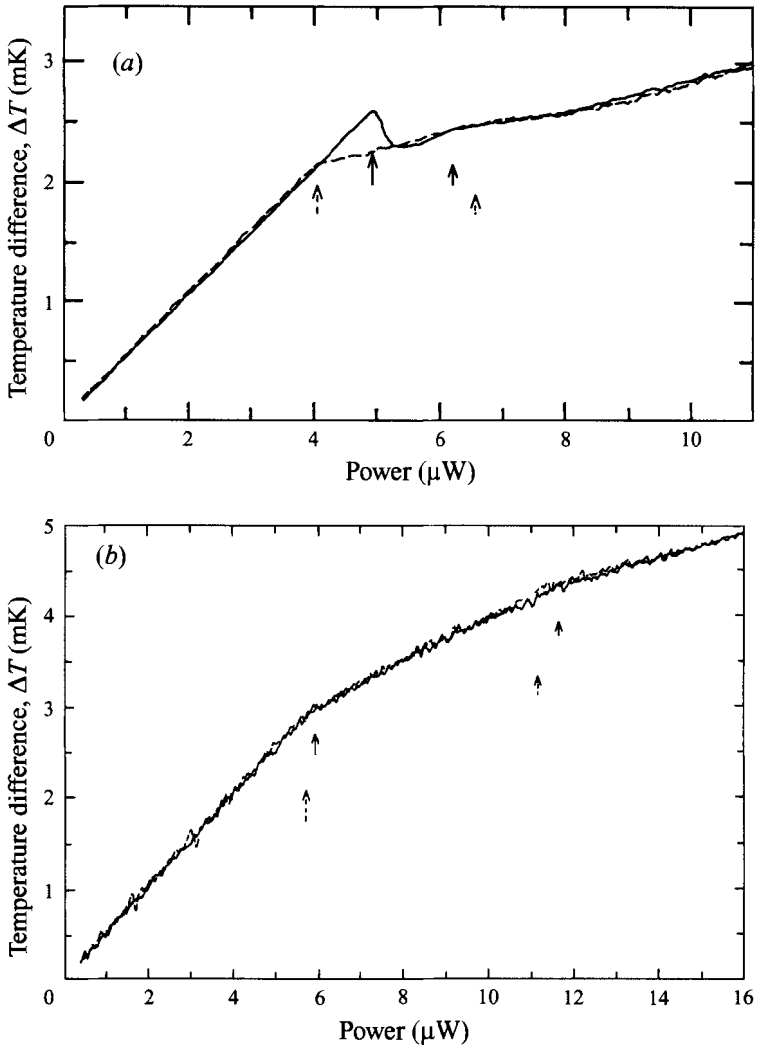

FIGURE 3. Heating curves for cell 1. Upper-boundary temperature set to (*a*) $T_1 = 2.161$ K, with dimensionless angular velocity $\Omega = 288.5$. (*b*) $T_4 = 2.233$ K with $\Omega = 542.6$. Solid line, heat-increasing sequence; dashed line, heat-decreasing sequence; long (short) solid arrows mark lower higher) convective transitions for heat increasing sequence; long (short) dashed arrows mark lower (higher) convective transitions for heat decreasing sequence.

& Meyer (1990) for β_c and β_T. The Rayleigh number was then calculated for a given ΔT using the definition above and with the fluid parameters evaluated at the molar concentration $X = 0.0222$ and the upper-boundary temperature appropriate to the heating ramp. The fluid parameters were not changing sufficiently rapidly with temperature at the temperatures at which the experiments were carried out to warrant correction to mid-plane temperatures and concentrations. To evaluate the fluid parameters at the temperatures and concentration of our experiments we constructed polynomial fits to the data given in the cited sources. A future publication is planned giving details of these fits, but a summary of all the fluid parameters relevant to these experiments is given in table 1.

In constructing this table the lack of directly measured data on the thermal diffusion ratio k_T over the temperature range at which our experiments were done makes it

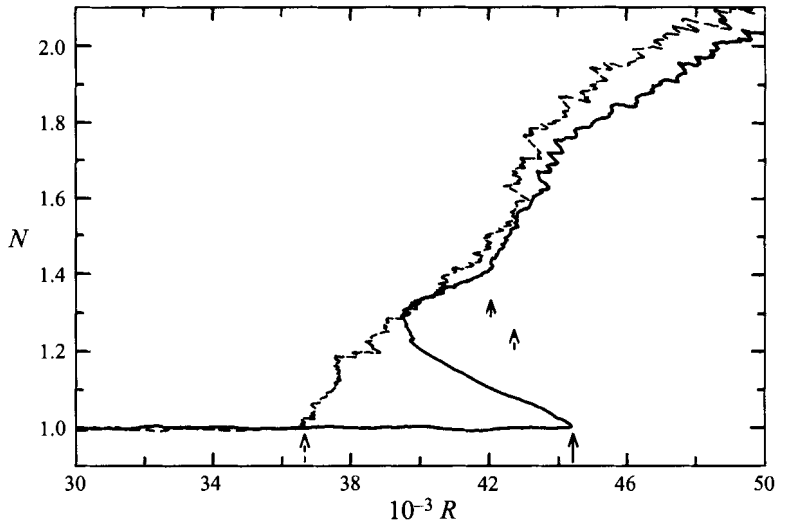

FIGURE 4. Dependence of Nusselt number N on Rayleigh number R for cell 1 for the heat-increasing (solid line) and heat-decreasing (dashed line) sequences shown in figure 3(*a*). Convective transitions are marked with the same symbols as in figure 3(*a*).

T (K)	β_T (10^{-2} K^{-1})	β_c	κ (10^{-4} Wcm^{-1} K^{-1})	k_T (10^{-3} K^{-1})	S	ν (10^{-4} cm^{-2} s^{-1})	D_T (10^{-4} cm^2 s^{-1})	L	σ
					$X = 0.0222$				
2.161	0.892	0.6832	1.466	9.12	-0.338	1.764	2.327	9.087×10^{-2}	0.7581
2.175	1.321	0.6915	1.401	4.06	-9.78×10^{-2}	1.807	2.555	7.555×10^{-2}	0.7072
2.2175	2.052	0.7042	1.375	0.275	-4.26×10^{-3}	1.919	3.138	5.344×10^{-2}	0.6117
2.233	2.235	0.7071	1.380	-0.214	3.03×10^{-3}	1.954	3.312	4.904×10^{-2}	0.5902
					$X = 0.0263$				
2.233	2.298	0.7065	1.379	0.081	-1.11×10^{-3}	1.964	3.371	4.518×10^{-2}	0.5827

TABLE 1. Dependence of fluid parameters on mixture ^3He molar concentration X and temperature T

difficult to compute S. This problem is discussed by Tuttle *et al.* (1991) who provide direct measurements at lower temperatures and at higher temperatures present the relationship $\epsilon^*(k_T = 0) = 1.49X$, where ϵ^* and T^* are the values of $(T_\lambda - T)/T_\lambda$ and T respectively for which k_T passes through zero. This relationship is based on the location of the codimension-two point in the convection experiments of Rehberg & Ahlers (1985) for their 0.03 molar percent mixture contained within a porous medium. Since we relied on the experimental data of Onions *et al.* (1990) to choose the four temperatures T_1 to T_4, it is more consistent for us to use their location of T_{CT} and T_b for our mixture. It is expected on theoretical grounds that the hydrodynamic tricritical point is located at a temperature T_b just lower than T^*. For example Schöpf & Zimmermann (1993) calculate $S_{CT} = -5 \times 10^{-4}$ and $S_b = -5 \times 10^{-6}$ for a mixture with fluid parameters not too dissimilar from those given in table 1. We therefore assumed that $T^* = T_b = 2.228$ K and $X = 0.0229$ as obtained by Onions *et al.* (1990), implying the relationship $\epsilon^* = 1.81X$. This relationship, together with the directly measured data

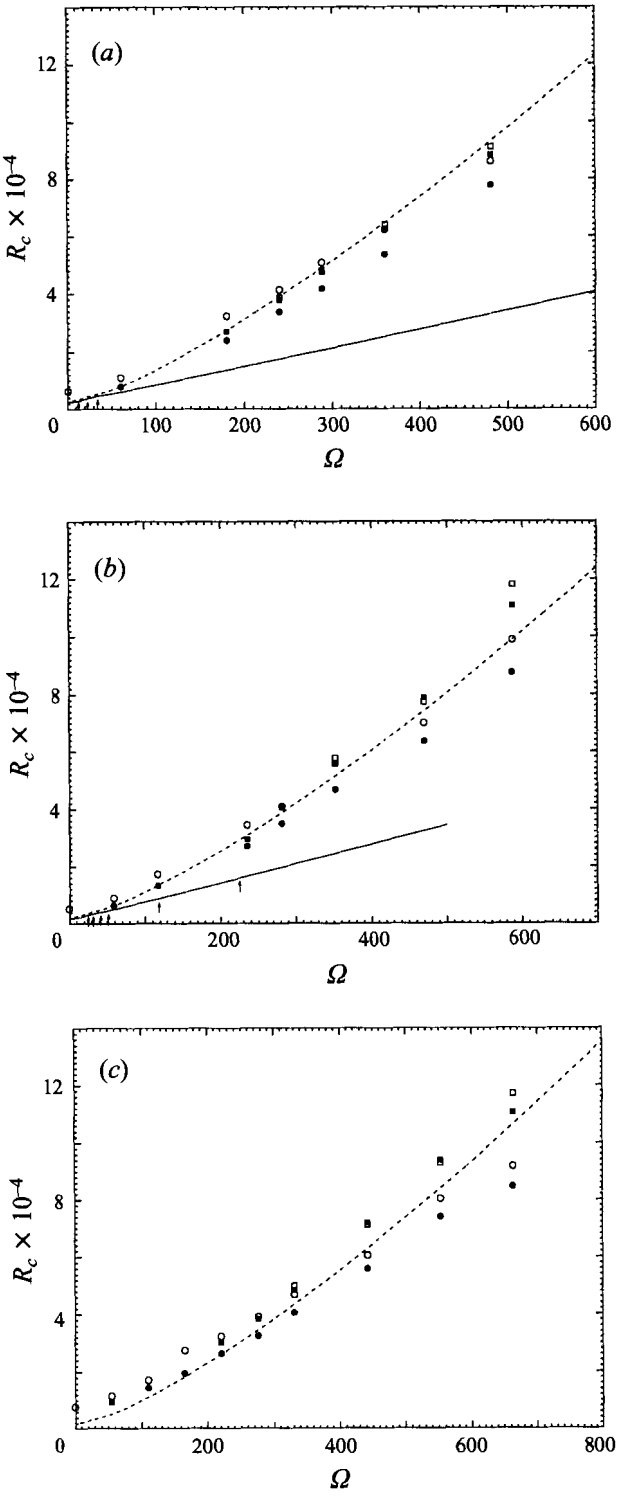

FIGURE 5(*a–c*). For caption see facing page.

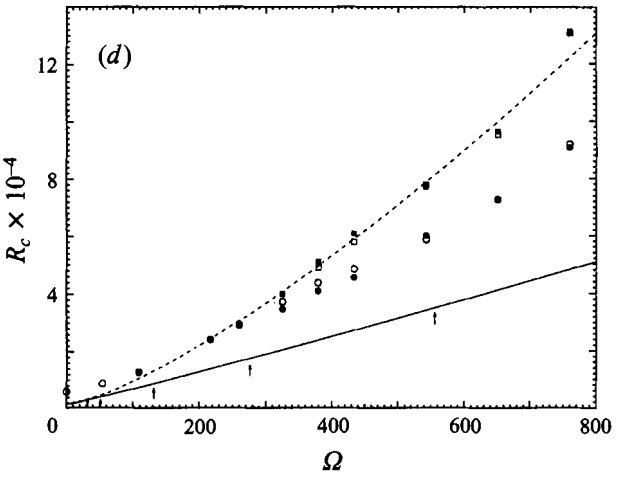

FIGURE 5. Dependence of critical Rayleigh number R_c on dimensionless angular velocity Ω for four different cell 1 upper-boundary temperatures T_U: (*a*) 2.161 K; (*b*) 2.175 K; (*c*) 2.218 K; (*d*) 2.233 K. Lower transition: ○, heat increasing; ●, heat decreasing. Upper transition: □, heat increasing; ■, heat decreasing. Individual random errors are not shown to avoid confusion but they are typically 10% for $\Omega = 0$, reducing to less than 1% for the highest angular velocities. Comparison with theory is as follows: ——, Net *et al.* (1995 and personal communication); ----, Ardron *et al.* (1992). The arrows indicate the angular velocities at which the mode number m changes in the calculations of Net *et al.* (1995).

on k_T at the lower temperatures allowed us to compute the parameters k_T and S presented in table 1. According to this fit the value of S_{CT} for the measurements of Onions *et al.* (1990) would be -1.1×10^{-2}.

To extract data on N from the experimental results at any particular value of R it was necessary to know what fraction of the heat developed in the lower boundary was flowing through the sidewalls. The total heat flow W_T through the cell can be written as a sum of bulk fluid (F) and wall (W) contributions:

$$W_T = (A_F/R_F + A_W/R_W)\Delta T, \tag{1}$$

where A and R are cross-sectional areas and thermal resistances respectively. In principle R_F contains a contribution from the Kapitza boundary resistance but since measurements in pure ^{4}He (Nakayama 1989) show that this is only about 0.03% of R_F it was neglected and provided the fluid is not convecting $R_F = d/\kappa$. By using the data sources on κ mentioned above we were able to calculate R_F, and then use the slopes $\Delta T/W_T$ of the heating curves in the non-convecting region and our knowledge of A_F and A_W to calculate the thermal resistance R_W of the walls from equation (1), which compared well with known data on the thermal conductivity of stainless steel. Once R_W was known, the wall contribution $A_W \Delta T/R_W$ could be subtracted from W_T to provide data on both W_F and the non-convecting contribution W_{NC} in the convecting region, permitting calculation of the Nusselt number $N = W_F/W_{NC}$.

4.2. *Experimental results for cell 1*

A common feature of all the heating curves is that at all four temperatures T_1 to T_4, below some critical angular velocity Ω_c which depends on temperature, only one change in gradient was visible over a heat flux range of about three times that at which the change occurs. For angular velocities greater than Ω_c a second change was observable at a higher heating power. The gradient change at the lower critical heating power is termed the low transition, while the second change is the higher transition.

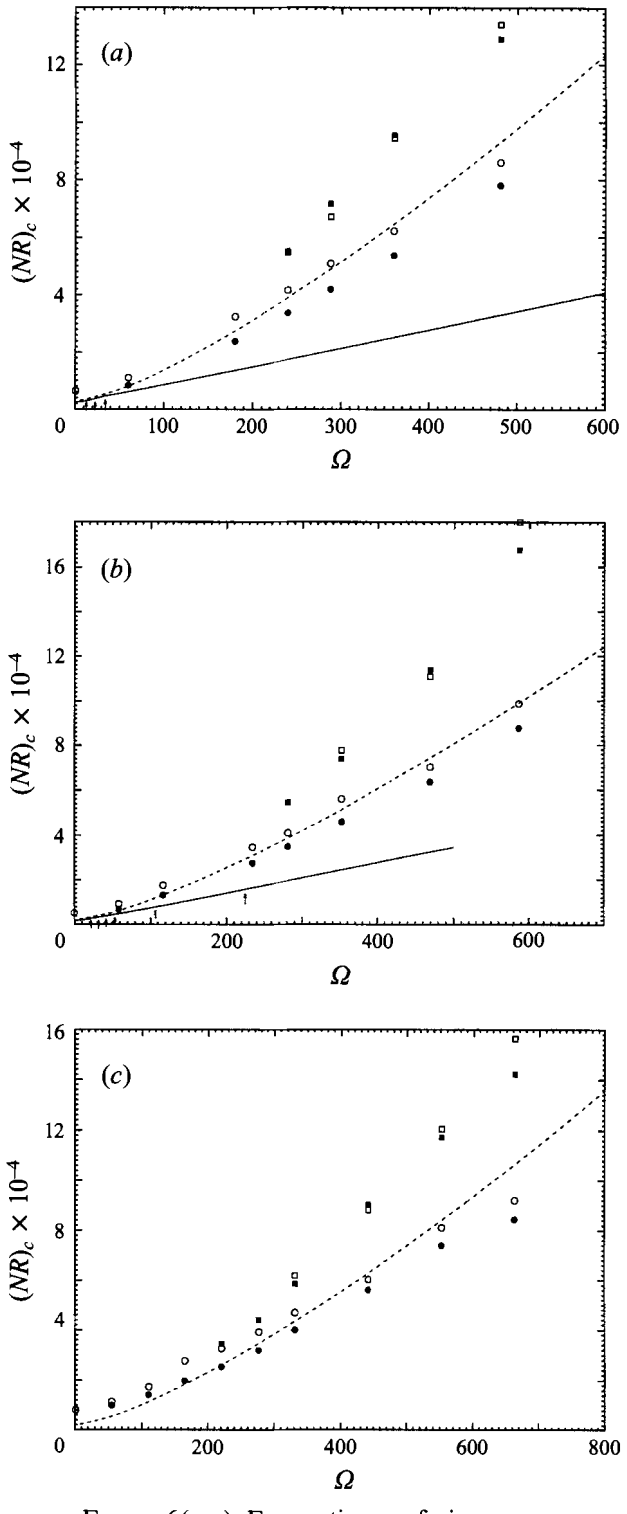

FIGURE 6(*a–c*). For caption see facing page.

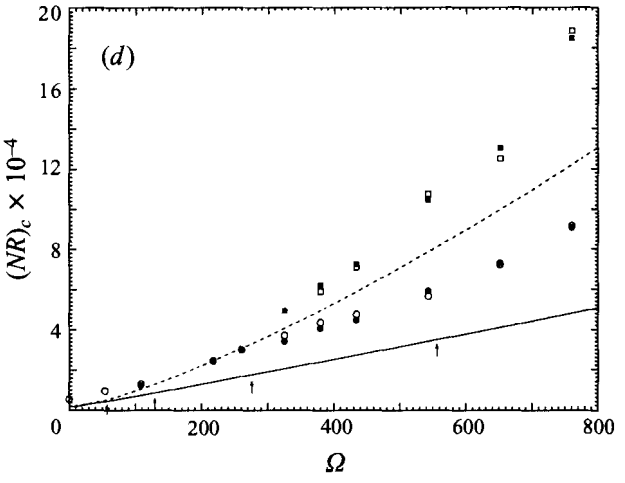

FIGURE 6. Dependence of critical dimensionless heat flux $(NR)_c$ on dimensionless angular velocity Ω for the four different cell 1 upper-boundary temperatures T_U; (*a*) 2.161 K; (*b*) 2.175 K; (*c*) 2.218 K; (*d*) 2.233 K. Symbols, theoretical lines and experimental errors are the same as for figure 5.

This behaviour is visible in figures 3(*a*) and 3(*b*) for which $\Omega > \Omega_c$ and has also been observed in pure ^{4}He by Lucas *et al.* (1983) and Pfotenhauer *et al.* (1984, 1987).

For the three temperatures T_1 to T_3, the bifurcation to the lower transition is backward, in the sense that for a heat-increasing sequence the temperature difference ΔT shows a fall with increasing heat flux just beyond the transition followed by a subsequent monotonic increase. This behaviour can be seen in figures 3(*a*) and 4. For a heat-decreasing sequence starting above the higher transition, ΔT decreases monotonically until the conduction state is regained without any observable sudden increase as might be expected if the system had passed through a saddle-node bifurcation point. Such an increase has been seen by Ahlers & Rehberg (1986) but the size of the jump in the Nusselt number ($\Delta N \sim 0.01$) is too small to be observable in our experiments. At T_4 the lower transition is forward within experimental error as can be seen from the heating curves in figure 3(*b*). The critical Rayleigh numbers at the lower and higher transitions are termed R_{c1} and R_{c2} respectively, while the Nusselt numbers are similarly N_{c1} and N_{c2}. Where a transition corresponded to a simple change in gradient of a heating curve, its location was determined by fitting straight lines on either side and determining their crossing point. Where a transition is clearly backward (e.g. the lower transition in figure 3*a*), its position was measured as that corresponding to the highest Rayleigh number local to the transition.

The dependence of the threshold Rayleigh number on dimensionless angular velocity Ω for these two transitions is shown in figure 5(*a–d*). Ω is defined by $\Omega = \Omega_D d^2/\nu$, where Ω_D is the dimensioned angular velocity, d is the cell height and ν the kinematic viscosity obtained from the polynomial fits described in the last section. For angular velocities below Ω_c the lower transition is not hysteretic within experimental error at the temperature T_4 and even above Ω_c the hysteresis is not great. The full extent of the hysteretic nature of the lower transition at the other temperatures is not too clear in figure 5(*a–c*) because these are Rayleigh number plots. The origin of the confusion can be seen from the heat-increasing sequence shown in figure 3(*a*) where the threshold Rayleigh number for the lower transition is higher than that of the higher transition. A clearer way of demonstrating the extent of the hysteresis is to plot the product of the Nussel number and Rayleigh number, NR, which is a dimensionless heat flux. This has

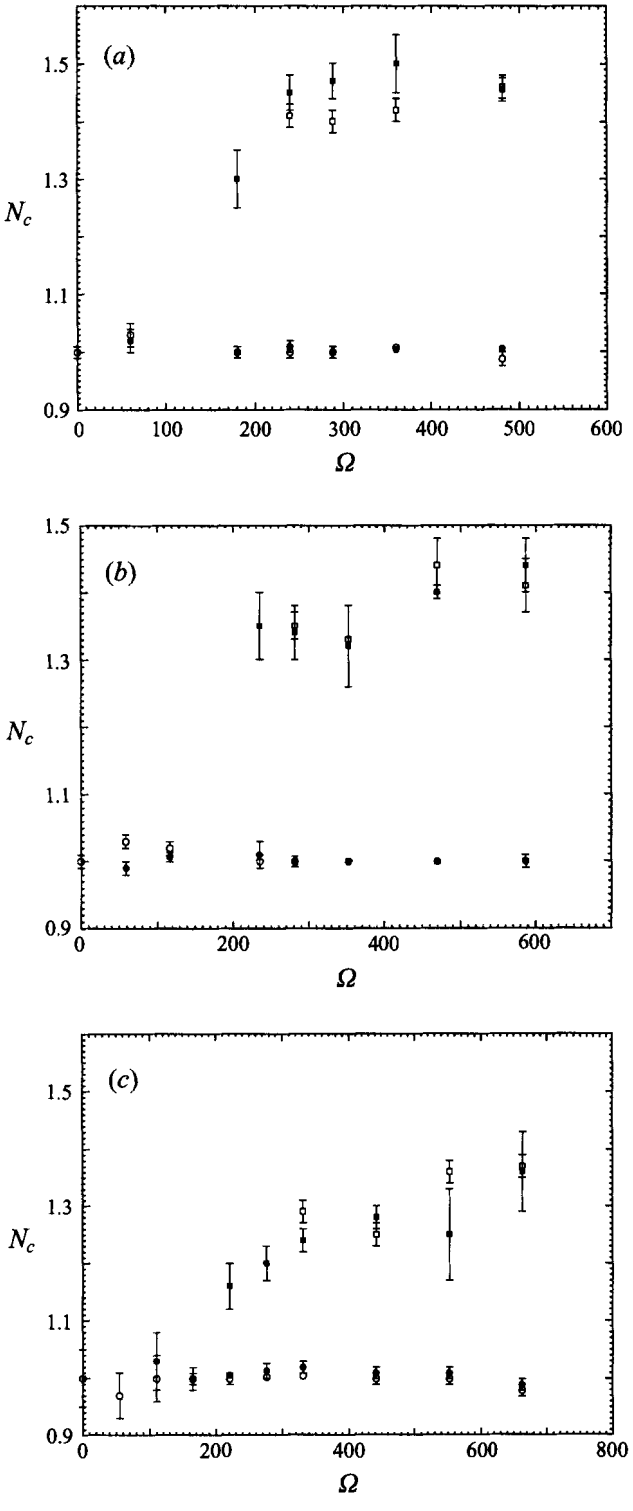

FIGURE 7(*a–c*). For caption see facing page.

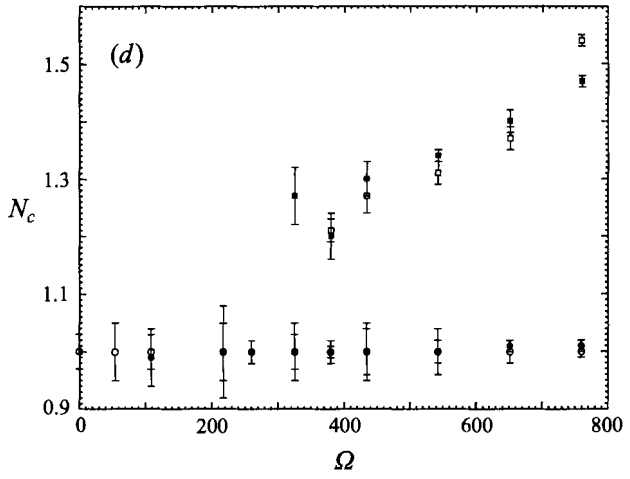

FIGURE 7. Dependence of critical Nusselt number N_c on dimensionless angular velocity Ω for the four different cell 1 upper boundary temperatures T_U: (*a*) 2.161 K; (*b*) 2.175 K; (*c*) 2.218 K; (*d*) 2.233 K. Symbols are the same as for figure 5.

been done in figure 6(*a–d*). The product $(NR)_c$ at either transition is calculated in practice from the relation

$$(NR)_c = (W_{Tc} - A_W \Delta T_c / R_W) g d^3 \beta_T / A_F R_F \nu D_T$$

rather than by direct multiplication of R_c and N_c, since the above method minimizes the experimental error. Direct heat transport data are also shown in the plots of Nusselt number against angular velocity in figure 7(*a–d*), while figure 8 is a plot of the drop δR in the Rayleigh number for all lower transitions that are backward. Finally table 2 contains data on Ω_c for each of the temperatures T_1 to T_4.

4.3. *Experiments with cell 2*

With cell 2, for which $\Gamma = 1$, we were seeking not only measurements of the angular velocity dependence of the Rayleigh number, but also information on the possible dependence of the convective-mode planform on the azimuthal angle, and their precession rates, to compare with the theoretical work of Goldstein *et al.* (1993, 1994) and Net *et al.* (1995). Thus we used the same ramping method described in §4.1 to provide Ω, R_c data, but in addition monitored the behaviour of the local probes in some cases. The observation of relaxation oscillations, found even when the system was not rotating, prompted us to perform some measurements of the time dependence of the outputs of the differential thermometer and the wall probes for fixed convective heat flux and rotation speed. All the experiments were performed at $T_4 = 2.233$ K to provide contact with the cell 1 measurements, even though the molar concentration $X = 0.0263$ used in cell 2 was a little higher. At this temperature, since $T_4 > T_b$, the mixture will differ little from pure ^{4}He, and the fluid parameters of the two mixtures are quite similar as can be seen from table 1.

The probes in the sapphire lower boundary deteriorated during the initial stages of thermal cycling between room temperature and 4.2 K that were required to get the system operational. By the time the rest of the experimental system was working they had failed completely. However, all three wall probes performed satisfactorily.

The larger vertical dimension of cell 2 compared with cell 1 allowed experiments to be performed at Rayleigh numbers and dimensionless angular velocities almost an order of magnitude greater because of the d^3 and d^2 scaling of these two parameters

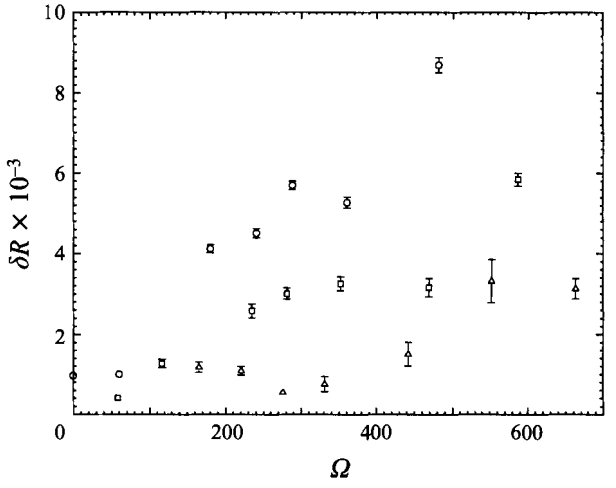

FIGURE 8. Dependence on dimensionless angular velocity Ω of the fall δR in the critical Rayleigh number for backward lower transitions taken from heat-increasing sequences with cell 1, for the three upper-boundary temperatures: ○, 2.161 K; □, 2.175 K; △, 2.218 K.

T (K)	Ω_c
2.161	190 ± 15
2.175	220 ± 20
2.2175	220 ± 20
2.233	250 ± 20

TABLE 2. Dependence on temperature T of the dimensionless critical angular velocity Ω_c above which two convective transitions are observed in cell 1, and below which only one transition is observed

respectively. While this allowed a wider exploration of (R, Ω)-space it had the disadvantage that the region explored with cell 2 only just overlapped that explored with cell 1. This arose because of the non-zero self-heating power being dissipated in the lower-boundary differential resistance sensor, R_{LD}. This provided a lower bound on the Rayleigh number which was only a little larger than the largest Rayleigh numbers employed with cell 1.

Cell 2 also differed from cell 1 in that the Vespel walls and stainless steel containing walls allowed of the order of 75% of the lower-boundary heating power to pass through them, in contrast with 30% in the case of cell 1. This contributed to making the change in the gradient of the heating curve at a convective transition relatively smaller than was the case with cell 1, making it more difficult to pick out the transitions. The temperature difference across the sapphire boundary in cell 2 was only about 0.01% of the temperature difference across the cell and was neglected.

4.4. *Experimental results for cell 2*

Figure 9(*a–c*) is a sample of the heating curves taken with the differential thermometer at dimensionless angular velocities 0, 853 and 1618 respectively. All the results obtained with cell 2 were for heat-increasing sequences. In the case of zero angular velocity, figure 9(*a*), small-amplitude (typically a few 100 μK) triangular waveform relaxation oscillations are noticeably superimposed on the curve. These are oscillations in time because the power is being ramped. A time series of the relaxation

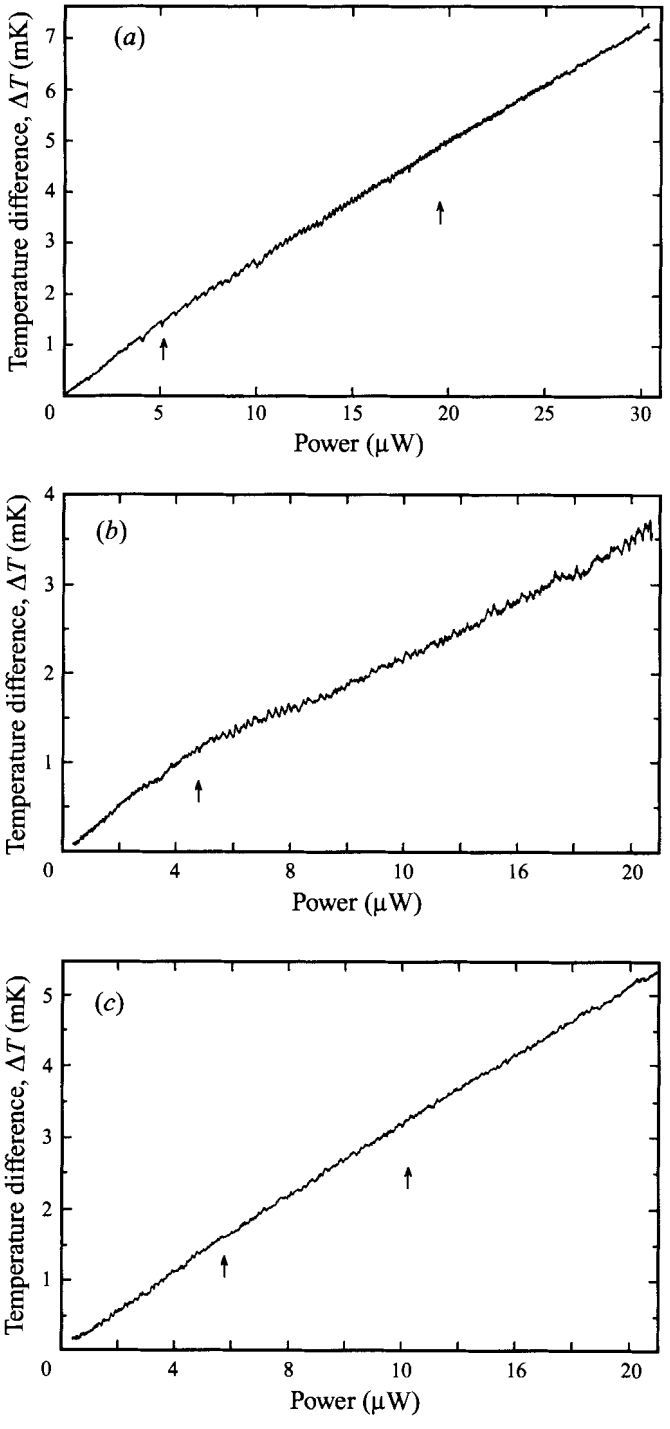

FIGURE 9. Heating curves for cell 2 with upper-boundary temperature T_U set at 2.233 K and with heat increasing for three different dimensionless angular velocities: (*a*) $\Omega = 0$; (*b*) $\Omega = 853$; (*c*) $\Omega = 1618$. Changes in gradient are marked with arrows.

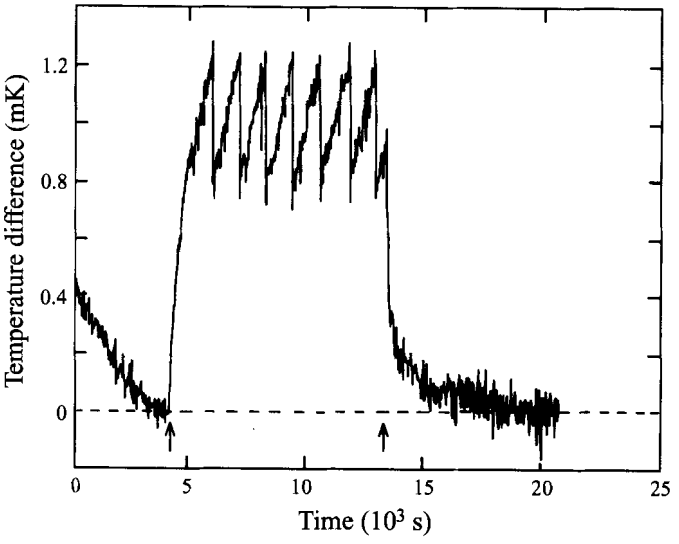

FIGURE 10. Time series of relaxation oscillations in cell 2 when not rotating, measured with one of the sidewall probes. A supercritical heat current was switched on at the time marked by the first arrow and then held constant until being switched off at the time marked by the second arrow. The rapid fall noticeable after each cycle occurs over a period of less than a second.

oscillations for the non-rotating cell is shown in figure 10. Relaxation oscillations in liquid helium in cylindrical containers have been reported before by, for example, Behringer, Gao & Shaumeyer (1983). Tuckerman & Barkley (1988) and Barkley & Tuckerman (1989) explain how relaxation oscillations can occur as radial travelling waves in a $\Gamma = 5$ cylinder containing pure fluid. Key features of their theory are that the sidewall thermal conductance should be high as measured by the dimensionless quantity

$$\mu = (\pi D_W / D_T) \tanh(\pi d_W / d),$$

where D_W and d_W are the thermal diffusivity and thickness respectively of the sidewalls, and that the Prandtl number should be greater than 0.7 for the oscillations to exist. The parameter μ takes the values 300 and 1.8×10^4 for cells 1 and 2 respectively, while according to the theory a value of at least 80 would ensure that time-dependent states take precedence over steady states. The Prandtl number at T_4 is just smaller than 0.7 but since our observations probably correspond to $\epsilon = (R - R_c)/R_c \sim 100$ and our Γ is 1 rather than 5 this may not rule out at least a similar mechanism to that of Barkley & Tuckerman (1989) for explaining our observations. Since it was apparent that the oscillations are a feature of the non-rotating cell and are not affected by rotation (except in instance iii below), a detailed separate report on the experiments performed on them is planned. Listed below, however, is a summary of the properties of the oscillations as determined by these experiments.

(i) The oscillations are present only when the power being dissipated in the lower boundary exceeds a critical value.

(ii) The frequency of the oscillations increases from zero monotonically with increasing boundary heating power, but is almost independent of angular velocity.

(iii) The amplitude of the oscillations is independent of heating power but decreases with increasing angular velocity and is undetectable above $\Omega = 350$.

(iv) The outputs of all three wall probes and the differential thermometer are always in phase regardless of angular velocity, indicating that the relaxation oscillation mode is independent of the aximuthal angle.

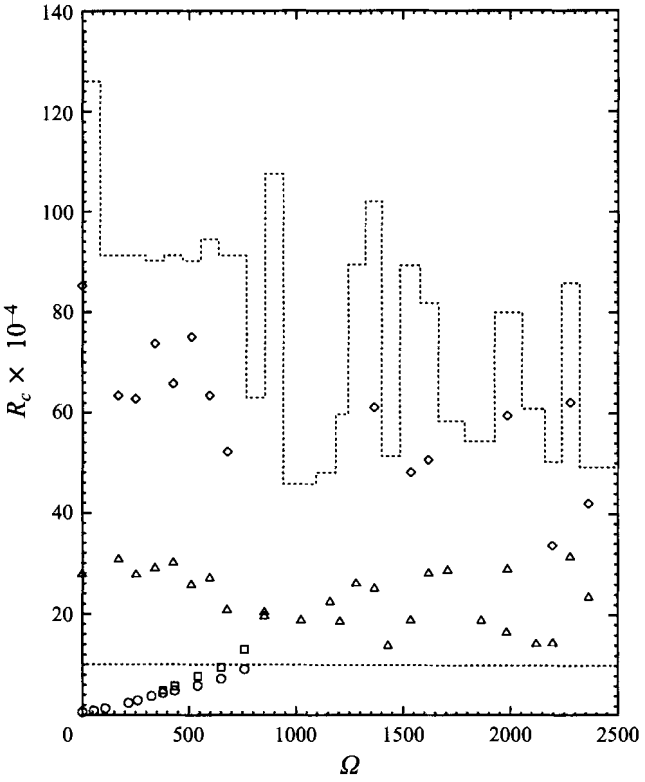

FIGURE 11. Dependence of critical Rayleigh number R_c on dimensionless angular velocity Ω for both cell 1 and cell 2. Only heat-increasing data are shown. Symbols are as follows: ○, cell 1, lower transition; □, cell 1, upper transition; △, cell 2, lower transition; ◇, cell 2, upper transition. The broken lines indicate the lowest and highest Rayleigh numbers explored with cell 2.

(v) The relaxation oscillations exist when the wall probes are not energized.

(vi) The rapid transition at the end of the ramp stage of each oscillation period takes place over a period of about 1 s which is about 5×10^{-4} vertical thermal diffusion times.

Heating curves 9(*a*) and 9(*c*) exhibit two changes in gradient. The change in gradient corresponding to the lower (higher) Rayleigh number we term the lower (upper) transition. Where relaxation oscillations were observable their appearance coincided with the lower transition. In the case of heating curve 9(*b*) there is only one change in gradient although there is a hint of another transition at a Rayleigh number lower than that corresponding to the main change in gradient. It was checked in a separate ramp at this angular velocity that no higher transition was visible up to a Rayleigh number of 1.07×10^6. For $870 < \Omega < 1300$ the gradients of the heating curves were about a factor of 0.7 smaller than those for $0 < \Omega < 700$ causing us in some cases to terminate unwittingly the heating ramp at Rayleigh numbers lower than those where the upper transition might be expected. For $1300 < \Omega < 1700$, the heating curves again had gradients similar to those for $0 < \Omega < 700$ with the exception of $\Omega = 1460$ which had a low gradient. For $\Omega > 1700$ the gradients varied between low and normal values with no discernible trend. For example for two separate heating curves with $\Omega = 2024$, one had a normal gradient and two transitions, the other had a low gradient and only one transition up to a Rayleigh number of 4×10^5.

The angular velocity dependence of the critical Rayleigh number for both the lower and upper transitions is summarized in figure 11. The regions of (R, Ω)-space explored

by the heating curves is shown. Also plotted are the cell 1 measurements at 2.233 K for comparison.

Time series data on the differential thermometer and sidewall probes were carried out at several fixed lower-boundary powers and at angular velocities 175 and 350. All four probes exhibited relaxation oscillations in phase with one another. There was no clear time dependence with phase shifts between the wall probes that might be expected if the convection mode had been a precessing wall mode of the type discussed by Goldstein *et al.* (1993, 1994) and Net *et al.* (1995).

5. Discussion

The angular velocity dependence of the critical Rayleigh number for cell 1, for which $\Gamma = 2.76$, is compared against theoretical calculations in figure 5(*a–d*). The theoretical calculations depicted by the broken line in figure 5 have been carried out by us using the sine-series scheme of Ardron *et al.* (1992), and consequently correspond to an unbounded rotating layer of the same height. The solid lines in figures 5(*a*), 5(*b*) and 5(*d*) are the more realistic calculations of Net *et al.* (1995) for a bounded layer of aspect ratio 2.76 and for the boundary conditions noted in §2. Note that those shown in figure 5(*b*) are not in Net *et al.* (1995) but have been kindly supplied to us separately by the authors of that paper.

The calculations of Net *et al.* (1995) shown in figures 5(*a*), 5(*b*) and 5(*d*) are intended to be relevant to a 2.22 molar percent mixture of ^{3}He in ^{4}He at the temperatures T_1, T_2 and T_4 respectively. Since the article by Net *et al.* (1995) was written, we have found it necessary to revise the fits described in §4.1 that allow us to compute the temperature and concentration dependence of the fluid parameters. The fluid parameters listed in table 1 have been computed from these revised fits, and all the experimental data and the sine-series calculations in this report have been prepared using these parameters. Thus the parameters in table 1 do not coincide exactly with those used by Net *et al.* (1995). The differences are not great, the main change being in the Lewis number L. The changes do not seem to affect the calculations of Net *et al.* (1995) seriously. They find that for stress-free boundary conditions and $\Omega = 500$ the effect of changing from $S = -0.323$, $L = 0.067$, $\sigma = 0.755$, to $S = -0.323$, $L = 0.09087$, $\sigma = 0.7581$ changes the critical Rayleigh number R_c by only 1.59% and Ω by 0.54% in the case of the $m = 0$ mode, and R_c by 5.3% and Ω by 0.50% in the case of the $m = 8$ mode and surmize that the changes in the more realistic case of rigid boundaries are comparable. The effect of the parameter changes on R_c as calculated by the sine-series technique is very similar: for example, at T_1, for $\Omega = 400$, R_c increases by 6%.

In comparing the results of the calculations with the experimental data for cell 1, it is important to recognize that all the calculation schemes are linear, and consequently refer to conduction/convection thresholds. We have assumed from the agreement between the data of Tuttle *et al.* (1991) and the mixture thermal conductivity obtained from the heating curve gradients below the lower transition, that the mixture is not convecting below this transition. Thus, assuming this to be the case, when there are two transitions it is the lower transition with the lower critical Rayleigh number that is to be compared with theory. Moreover when the bifurcation is backward, only the experimental data for heat-increasing sequences are directly comparable with the calculations.

The calculations of Net *et al.* (1995), performed for finite aspect ratio Γ, allow for the possibility that the threshold state can be a non-axisymmetric precessing wall mode. These states have lower critical Rayleigh numbers than the axisymmetric body

modes. Since the unbounded layer can only support body modes, these features are not taken into account in our calculations using the sine-series scheme. Nevertheless, we have included them since, except at low angular velocities, they serve as a useful upper bound to the expected critical Rayleigh numbers.

It can be seen from figure 5(*a–d*) that the experimental data for cell 1 on the lower-transition heat-increasing critical Rayleigh numbers lie between the unbounded layer calculations and the calculations of Net *et al.* (1995), provided the angular velocity is sufficiently large. At low angular velocities the experimental data lie above both theoretical calculations. In particular the experimental data at $\Omega = 0$ lie above the calculations of Mercader *et al.* (1995) for a non-rotating ^{3}He–^{4}He mixture contained in a cylinder of aspect ratio 2.76. These authors have computed the critical Rayleigh number for the conduction/convection thresholds for fluid parameters intended to be relevant to temperatures T_1 and T_4, but which differ from the values assumed by us in this paper by small amounts for the reasons given earlier. Assuming $S = -0.32$ at T_1 and $S \approx 0$ at T_4, their calculations yield $R_c = 2600$ at T_1 and $R_c \approx 1800$ at T_4. The experimental values of R_{c1} when $\Omega = 0$ for heat-increasing sequences at T_1 and T_4 are 5750 ± 500 and 5200 ± 520 respectively. While the experimental errors on these measurements are large because cell 1 was not designed for measuring these small Rayleigh numbers accurately, the theoretical values above lie outside the range permitted by experimental error.

It is a feature of the models of Goldstein *et al.* (1992, 1993) and Net *et al.* (1995), that the mode possessing the lowest critical Rayleigh number changes with angular velocity, so that body modes with small or zero azimuthal mode number m are preferred for small Ω, while non-axisymmetric wall modes with higher values of m are preferred at higher Ω. The cross-over between these two kinds of flow pattern occurs near $\Omega = 30$ and is responsible for a pronounced cusp at this angular velocity in their calculated (R_c, Ω)-plots. Cusps are present in the calculated data whenever the mode number changes but these are much weaker and are not likely to be observable although their locations are indicated on figures 5(*a*), 5(*b*) and 5(*d*). The branch to two transitions observed at the angular velocities given in table 2 is a possible candidate for the body-mode to wall-mode transition, but occurs at values of Ω between 200 and 300. The transition at R_{c2} observed in our experiments when Ω exceeds this critical value, and also by Lucas *et al.* (1983) and Pfotenhauer *et al.* (1984, 1987) is not well understood. A similar aperiodic higher transition has been observed by Zhong, Ecke & Steinberg (1991) and Zhong *et al.* (1993) in rotating water.

The extent to which the experimental data on R_c lie above the theoretical calculations of Net *et al.* (1995) is too large to be explained by experimental error. One possible reason may be that the vertical temperature gradient at the sidewalls is affected by the thermal conductivity of the sidewalls, which in the case of cell 1 is about an order of magnitude larger than that of the fluid mixture. Thus it may be necessary to take into account the boundary condition on the vertical temperature gradient at the sidewalls in the theory. In convection experiments on water confined in a non-rotating cylindrical container with aspect ratio 10, Meyer, Ahlers & Cannell (1991) observed substantially different convection flow patterns when the sidewall thermal properties were changed. Another possibility (E. Knobloch 1995, personal communication) lies in the thermal properties of the wall modes, which in the theory are the preferred states over most of the angular velocity range covered by the experiments. Since in these modes most of the flow takes place close to the walls, the convective heat flux for wall modes may be small compared with that for body modes. Thus the Nusselt number may not change substantially until the wall mode loses stability to a body mode, which

might be expected to occur at a critical Rayleigh number corresponding to the unbounded layer. If this explanation is correct the experimental data on R_c should lie close to the sine-series calculations, which is the case for T_1, T_2 and T_3, but not for T_4.

Net *et al.* (1995) note the interesting effect that for sufficiently negative S, about -0.3, and for angular velocities greater than about 250, the critical Rayleigh number is depressed below its value when $S = 0$, all the other fluid parameters remaining the same. Although figures 5(*a*) and 5(*d*) correspond respectively to $S = -0.3$ and $S \approx 0$, the other fluid parameters are also different, as can be seen from table 1. It is not therefore straightforward to look for this effect and with the present data it does not seem possible to detect it.

It is clear from the cell 1 data that the hysteretic behaviour for temperatures below T_b and non-hysteretic behaviour above T_b still exists when the fluid rotates. Since only four temperatures were investigated the angular velocity dependence of T_b cannot be known beyond the extent that it still lies between T_3 and T_4 up to $\Omega = 700$. There are probably insufficient different temperatures at which data were taken to be able to extract information on the angular velocity dependence of the codimension-two point.

The experimental data for cell 2 show greater experimental scatter than was obtained for cell 1. Nevertheless, as can be seen from figure 11, the contrast between the angular-velocity-dependent data for cell 1 and the almost angular-velocity-independent data for cell 2 is marked. The more complicated structure of cell 2 and the increased experimental error did not permit us to calculate the fluid thermal conductivity below the lower transition to any degree of precision. Consequently it was not possible to infer whether the fluid in the cell below the lower transition was conducting. It seems likely to us, however, that the lower and upper transitions correspond to the flow state changing from one convective mode to another. At the highest angular velocity ($\Omega = 950$) for which Net *et al.* (1995) give data for no-slip boundary conditions and $\Gamma = 2.76$ the conduction-to-convection threshold is predicted to occur at a Rayleigh number of 6.05×10^4 for the non-axisymmetric state with azimuthal mode number $m = 12$. This Rayleigh number is equivalent to $\Delta T_c = 0.038$ mK which is a factor of 5 smaller than is detectable in the experiments. The experimental data are suggestive of the kind of transition diagram in (R_c, Ω)-space such as figure 7(*a*) of Goldstein *et al.* (1994), with the increases in fluid conductance in particular ranges of Ω corresponding to mode cross-over. The difference between the angular velocity dependence of the critical Rayleigh number as obtained from the two cells may also be affected by the difference in the thermal properties of the materials used for the sidewalls. For stainless steel (the sidewall material of cell 1), the thermal conductivity, specific heat capacity and density are about 10^{-3} W cm^{-1} K^{-1}, 10^{-3} J g^{-1} K^{-1} and 8 g cm^{-3} respectively at 2.2 K. Thus at this temperature the thermal diffusivity of stainless steel is about 0.1 cm^2 s^{-1}. For Vespel-22 (the sidewall material used for cell 2), the thermal conductivity and density are about 8.5×10^{-5} W cm^{-1} K^{-1} and 1.6 g cm^{-3} respectively at 2.2 K. The specific heat capacity of Vespel-22 does not seem to have been measured at 2.2 K but must be similar to that of graphite which is 2.8×10^{-5} J g^{-1} K^{-1}. Making this assumption the thermal diffusivity of Vespel-22 at 2.2 K is about 2 cm^2 s^{-1}. Thus both the thermal conductivities and to a lesser extent the thermal diffusivities are substantially different for the two materials, and the thermal diffusivities for both materials are much larger than that of the mixture.

Although the expected precessional-mode temperature variations were not detected with the local probes, it is possible that they were too small to be observed. Despite the probes being sensitive enough to detect changes of 10 μK, in the geometry of cell 2 this corresponds to a change in Rayleigh number of 1600. In the experiments with cell 2,

it is likely that the fluid was always in a convecting state in which nonlinear terms in the equations of motion were important.

The unexpected heating curve gradient differences observed for cell 2 are possibly a result of the fluid sometimes achieving a more efficient heat transfer state accessible only if the cell experiences a thermal shock resulting from external noise. An example of this is recorded by Warkentin *et al.* (1980).

This work was supported by EPSRC grants GR/H 95075 and GR/F 22036. One of us (J.K.B.) gratefully acknowledges the award of a EPSRC Visiting Research Fellowship. We acknowledge many helpful discussions with Dr E. Knobloch and Professor H. E. Hall.

REFERENCES

AHLERS, G. & REHBERG, I. 1986 Convection in a binary mixture heated from below. *Phys. Rev. Lett.* **56**, 1373–1376.

ANTORANZ, J. C. & VELARDE, M. G. 1978 Soret-driven convective instability with rotation. *Phys. Lett.* **65A**, 377–379.

ANTORANZ, J. C. & VELARDE, M. G. 1979 Thermal diffusion and convective stability: The role of uniform rotation of the container. *Phys. Fluids* **22**, 1038–1043.

ARDRON, M. R., LUCAS, P. G. J., ONIONS, T., TERRETT, M. D. J. & THURLOW, M. S. 1990 Rotating cryogenic platform. *Physica* B **165/166**, 55–56.

ARDRON, M. R., LUCAS, P. G. J. & STEIN, N. D. 1992 Exact calculation of convection thresholds in rotating binary liquid mixtures. *Phys. Fluids* **A4**, 664–670.

BARKLEY, D. & TUCKERMAN, L. S. 1989 Traveling waves in axisymmetric convection: the role of sidewall conductivity. *Physica* D **37**, 288–294.

BEHRINGER, R. P., GAO, H. & SHAUMEYER, J. N. 1983 Time dependence in Rayleigh–Bénard convection with a variable cylindrical geometry. *Phys. Rev. Lett.* **50**, 1199–1202.

BHATTACHARJEE, J. K. 1988*a* Preferred patterns in convection in rotating binary mixtures. *Phys. Rev.* A **37**, 1368–1370.

BHATTACHARJEE, J. K. 1988*b* Convection in rotating binary mixtures. I. Thresholds. *Phys. Fluids* **31**, 2456–2461.

BHATTACHARJEE, J. K. 1988*c* Convection in rotating binary mixtures. II. Küppers–Lortz instability. *Phys. Fluids* **31**, 2462–2466.

BHATTACHARJEE, J. K. 1989 Convection in rotating binary mixtures. III. Galerkin models. *Phys. Fluids* A **1**, 1938–1948.

BRAND, M. R., HOHENBERG, P. C. & STEINBERG, V. 1984 Codimension-2 bifurcations for convection in binary fluid mixtures. *Phys. Rev.* A **30**, 2548–2561.

BUELL, J. C. & CATTON, I. 1983 Effect of rotation on the stability of a bounded cylindrical layer of fluid heated from below. *Phys. Fluids* **26**, 892–896.

CLEVER, R. M. & BUSSE, F. H. 1979 Nonlinear properties of convection rolls in a horizontal layer rotating about a vertical axis. *J. Fluid Mech.* **94**, 609–627.

CLUNE, T. & KNOBLOCH, E. 1992 Mean flow suppression by endwalls in oscillatory binary fluid convection. *Physica* D **61**, 106–112.

DELONG, L. E., SYMKO, O. G. & WHEATLEY, J. C. 1971 Continuously operating ^{4}He evaporation refrigerator. *Rev. Sci. Instrum.* **42**, 147–150.

ECKE, R. E., ZHONG, F. & KNOBLOCH, E. 1992 Hopf bifurcation with broken reflection symmetry in rotating Rayleigh-Bénard convection. *Europhys. Lett.* **19**, 177–182.

GAO, H. & BEHRINGER, R. P. 1986 Convective instabilities of a normal liquid ^{3}He–^{4}He mixture. *Phys. Rev.* A **34**, 697–700.

GASPARINI, F. & MOLDOVER, M. R. 1975 Specific heat of ^{4}He and ^{3}He–^{4}He mixtures at their λ transition. *Phys. Rev.* B **12**, 93–113.

GESTRICH, D., WALSWORTH, R. & MEYER, H. 1984 Transport properties in ^{3}He–^{4}He mixtures near the superfluid transition. *J. Low Temp. Phys.* **54**, 37–61.

GOLDSTEIN, H. F. & KNOBLOCH, E. 1991 Linear stability of rotating Rayleigh–Bénard convection in a finite cylinder. *Bull. Am. Phys. Soc.* **36**, 2649–2650.

GOLDSTEIN, H. F., KNOBLOCH, E., MERCADER, I. & NET, M. 1993 Convection in a rotating cylinder. Part 1. Linear theory for moderate Prandtl numbers. *J. Fluid Mech.* **248**, 583–604.

GOLDSTEIN, H. F., KNOBLOCH, E., MERCADER, I. & NET, M. 1994 Convection in a rotating cylinder. Part 2. Linear theory for low Prandtl numbers. *J. Fluid Mech.* **262**, 293–324.

KAKIZAKI, A. & SATOH, T. 1976 Thermodynamic properties of ^{3}He–^{4}He mixtures near T_λ. *J. Low Temp. Phys.* **24**, 67–84.

KIERSTEAD, H. A. 1976 Dielectric constant, molar volume, and phase diagram of saturated liquid ^{3}He–^{4}He mixtures. *J. Low Temp. Phys.* **24**, 497–512.

KOLODNER, P. 1994 Stable, unstable, and defected confined states of traveling-wave convection. *Phys. Rev.* E **50**, 2731–2755.

LEE, G. W. T., LUCAS, P. & TYLER, A. 1983 Onset of Rayleigh–Bénard convection in binary liquid mixtures of ^{3}He in ^{4}He. *J. Fluid Mech.* **135**, 235–259.

LUCAS, P. & DONNELLY, J. A. 1981 Computer-automated ratio transformer bridge. *Rev. Sci. Instrum.* **52**, 582–584.

LUCAS, P. G. J., PFOTENHAUER, J. M. & DONNELLY, R. J. 1983 Stability and heat transfer of rotating cryogens. Part 1. Influence of rotation on the onset of convection in liquid ^{4}He. *J. Fluid Mech.* **129**, 251–264.

LUCAS, P. G. J., THURLOW, M. S., ARDRON, M. R., BHATTACHARJEE, J. K., KERSHAW, B. J., TERRETT, M. D. J. & WOODCRAFT, A. L. 1994 Rayleigh–Bénard convection in rotating liquid ^{3}He–^{4}He mixtures. *Physica* B **194/196**, 841–842.

MERCADER, I., NET, M. & KNOBLOCH, E. 1995 Binary fluid convection in a cylinder. *Phys. Rev.* E **51**, 339–350.

MEYER, C., AHLERS, G. & CANNELL, D. S. 1991 Stochastic influences on pattern formation in Rayleigh-Bénard convection: ramping experiments. *Phys. Rev.* A **44**, 2514–2537.

NAKAYAMA, T. 1989 Kapitza thermal boundary resistance and interactions of helium quasiparticles with surfaces. In *Progress in Low Temperature Physics*, Vol. 12 (ed. D. Brewer), pp. 115–194. North-Holland.

NET, M., MERCADER, I. & KNOBLOCH, E. 1995 Binary fluid convection in a rotating cylinder. *Phys. Fluids* **7**, 1553–1567.

ONIONS, T., ARDRON, M. R., LUCAS, P. G. J., TERRETT, M. D. J. & THURLOW, M. S. 1990 Codimension-two and hydrodynamic tricritical points in ^{3}He–^{4}He mixtures. *Physica* B **165/166**, 521–522.

PACKARD, R. E. & WILLIAMS, G. A. 1974 A triaxial rotating vacuum seal. *Rev. Sci. Instrum.* **45**, 1179.

PEARLSTEIN, A. J. 1981 Effect of rotation on the stability of a doubly diffusive fluid layer. *J. Fluid Mech.* **103**, 389–412.

PFOTENHAUER, J. M., LUCAS, P. G. J. & DONNELLY, R. J. 1984 Stability and heat transfer of rotating cryogens. Part 2. Effects of rotation on heat-transfer properties of convection in liquid ^{4}He. *J. Fluid Mech.* **145**, 239–252.

PFOTENHAUER, J. M., NIEMELA, J. J. & DONNELLY, R. J. 1987 Stability and heat transfer of rotating cryogens. Part 3. Effects of finite geometry and rotation on the onset of convection. *J. Fluid Mech.* **175**, 85–96.

REHBERG, I. & AHLERS, G. 1985 Experimental observation of a codimension-two bifurcation in a binary mixture. *Phys. Rev. Lett.* **55**, 500–503.

RYSCHKEWITSCH, M. G. & MEYER, H. 1979 Concentration susceptibility of ^{3}He–^{4}He mixtures near the superfluid transition. *J. Low Temp. Phys.* **35**, 103–133.

SCHÖPF, W. & ZIMMERMANN, W. 1993 Convection in binary fluids: Amplitude equations, codimension-2 bifurcation, and thermal fluctuations. *Phys. Rev.* E **47**, 1739–1764.

SHERMAN, R. H., SYDORIAK, S. G. & ROBERTS, T. R. 1964 The 1962 ^{3}He scale of temperatures. IV. Tables. *J. Res. Natl. Bureau of Standards A. Physics and Chemistry* **68A**, 579–588.

SULLIVAN, T. & AHLERS, G. 1988*a* Hopf bifurcation to convection near the codimension-two point in a ^{3}He–^{4}He mixture. *Phys. Rev. Lett.* **61**, 78–81.

SULLIVAN, T. & AHLERS, G. 1988*b* Nonperiodic time dependence at the onset of convection in a binary liquid mixture. *Phys. Rev.* A **38**, 3143–3146.

SULLIVAN, T. S., STEINBERG, V. & ECKE, R. E. 1993 Thermal convection and thermal conductivity of nondilute ^{3}He–^{4}He mixtures. *J. Low Temp. Phys.* **90**, 343–354.

SYDORIAK, S. G. & ROBERTS, T. R. 1960 Vapour pressure of ^{3}He–^{4}He mixtures. *Phys. Rev.* **118**, 901–912.

TAKADA, T. & WATANABE, T. 1980 Specific heat near the lambda point in ^{4}He and ^{3}He–^{4}He mixtures: test of universality of the critical exponent and the amplitude ratio, and observation of the critical-tricritical crossover effect. *J. Low Temp. Phys.* **41**, 221–241.

TUCKERMAN, L. S. & BARKLEY, D. 1988 Global bifurcation to traveling waves in axisymmetric convection. *Phys. Rev. Lett.* **61**, 408–411.

TUTTLE, J., ZHONG, F. & MEYER, H. 1991 Thermal transport properties in the normal phase of dilute ^{3}H–^{4}He mixtures. *J. Low Temp. Phys.* **83**, 283–305 (and erratum **98**, 1995, 631–633).

WANG, S., HOWALD, C. & MEYER, H. 1990 Shear viscosity of liquid ^{4}He and ^{3}He–^{4}He mixtures, especially near the superfluid transition. *J. Low Temp. Phys.* **79**, 151–187.

WARKENTIN, P. A., HAUCKE, H. J., LUCAS, P. & WHEATLEY, J. C. 1980 Stationary convection in dilute solutions of ^{3}He in superfluid ^{4}He. *Proc. Natl. Acad. Sci.* **77**, 6983–6987.

WEBELER, R. W. H. & ALLEN, G. 1972 Lambda-point measurement of $\eta\rho_n$ for pure ^{3}He and for three ^{3}He–^{4}He mixtures. *Phys. Rev.* A **5**, 1820–1827.

WHITE, G. K. 1979 *Experimental Techniques in Low Temperature Physics.* Clarendon.

ZHONG, F., ECKE, R. E. & STEINBERG, V. 1991 Asymmetric modes and the transition to vortex structures in rotating Rayleigh–Bénard convection. *Phys. Rev. Lett.* **67**, 2473–2476.

ZHONG, F., ECKE, R. E. & STEINBERG, V. 1993 Rotating Rayleigh–Bénard convection: asymmetric modes and vortex states. *J. Fluid Mech.* **249**, 135–159.

ZHONG, F., TUTTLE, J. & MEYER, H. 1990 Transport properties in the superfluid phase of dilute ^{3}He–^{4}He mixtures near T_λ. *J. Low Temp. Phys.* **79**, 9–54.